

Energy-compatible and spectrum-compatible (ECSC) ground motion simulation using wavelet packets

Duruo Huang and Gang Wang^{*,†}

Department of Civil and Environmental Engineering, Hong Kong University of Science and Technology, Clear Water Bay, Kowloon, Hong Kong

SUMMARY

A stochastic ground-motion simulation and modification technique is developed to generate energy-compatible and spectrum-compatible (ECSC) synthetic motions through wavelet packet characterization and modification in both frequency and time domains. The ECSC method significantly advances traditional spectral matching approaches, because it generates ground motions that not only match the target spectral accelerations, but also match Arias intensity build-up and significant durations. The great similarity between the ECSC simulated motions and the actual recorded motions is demonstrated through one-to-one comparison of a variety of intensity measures. Extensive numerical simulations were also performed to validate the performance of the ECSC ground motions through nonlinear analyses of elasto-plastic oscillators. The ECSC method can be easily implemented in the generalized conditional intensity measure framework by directly simulating a set of motions following a targeted distribution of multiple intensity measures. Therefore, the ECSC method has great potential to be used in performance-based earthquake design and analysis. Copyright © 2017 John Wiley & Sons, Ltd.

Received 23 March 2016; Revised 29 September 2016; Accepted 7 February 2017

KEY WORDS: synthetic ground motions; frequency- and time-domain modification; wavelet packet analysis

1. INTRODUCTION

Performance-based earthquake design often requires evaluation of structural responses using earthquake ground motion acceleration time histories. However, the number of available strong-motion data is often insufficient. In regions of active seismicity, large-magnitude earthquakes at design levels have very low probabilities of occurrence. Ground motion data are particularly sparse in regions of low-to-moderate seismicity such as the Eastern United States, Australia and Hong Kong. In order to analyze the seismic performance of structures, ground-motion time histories need to be selected and modified from recorded strong-motion database [1, 2], or numerically generated using either deterministic or stochastic approaches. In this paper, stochastic simulation refers to a class of methods that directly generate ground-motion time histories using a few empirically calibrated parameters [3–11]. Comparing with physics-based deterministic numerical approaches [12, 13] and hybrid methods [14], stochastic simulation does not consider the physics of fault rupture process and wave propagation phenomena that require extensive computation. Yet, stochastic methods are particularly cost effective for design purposes. It is possible to generate thousands of ground-motion time histories within a few hours using stochastic simulation.

*Correspondence to: Gang Wang, Department of Civil and Environmental Engineering, Hong Kong University of Science and Technology, Clear Water Bay, Kowloon, Hong Kong.

†E-mail: gwang@ust.hk

Ground motion effects on structures are usually represented by spectral accelerations, which reflect both amplitude and frequency content of a ground motion [15–18]. For design purposes, ground motions can be stochastically simulated to be compatible with a prescribed response spectrum. A notable example is SIMQKE, which iteratively adjusts the Fourier components of a modulated Gaussian random process until the spectral amplitudes of the generated motion closely match a target spectral shape [19]. One of the limitations of the above procedure is the frequency content of the accelerograms cannot vary with time. The simulation is also not related to any specific seismological environment.

However, the generation of the spectrum-compatible time histories is an ‘ill posed’ problem [20], in which more than one ground-motion time history may be developed to match a target response spectrum. Yet, these time histories may have totally different characteristics such as cumulative energy, duration as well as nonstationary characteristics. These parameters have been found to be important in the analysis of certain types of structures. For example, Chandramohan *et al.* [21, 22] demonstrated that ground-motion duration is important in risk assessments of structural collapse; Wang [23] showed that the Arias intensity (I_a), in addition to spectral acceleration, is critical for estimating seismic slope displacements.

Therefore, rigorous ground-motion selection and modification process requires consideration of multiple intensity measures (IMs) collectively. Following this line, a generalized conditional intensity measure (GCIM) framework has been established for ground-motion selection [24–26]. The method is an extension of the conditional mean spectrum concept [27] and allows for selecting ground motions conditional on multivariate IMs that are identified important in seismic response analyses. The accuracy of the GCIM framework has been evaluated using nonlinear time history analysis of simple structures [28, 29], which highlights the significance of the conditioning multiple IMs in ground-motion selection process. However, none of the existing stochastic methods can directly generate synthetic ground motions targeting at these multiple IMs.

In this study, a stochastic simulation and modification method is proposed to generate synthetic ground motions whose response spectrum and I_a build-up process are compatible with specified targets, resulting in so-called energy-compatible and spectrum-compatible (ECSC) ground motions. The stochastic model adopted in this study was initially proposed by Yamamoto and Baker [30] to simulate ground motions using wavelet packet transform (WPT). Compared with other wavelet-based methods, WPT has basis functions that are orthogonal and localized in time and frequency domains. The salient feature allows for ground-motion time histories to be flexibly adjusted in frequency domain and time domain simultaneously. Therefore, their response spectrum and cumulative energy can be modified. The authors will conduct systematic studies to validate the simulated ECSC motions against real recorded motions using nonlinear oscillators. As the current study can be regarded as stochastic modeling conditioned on given seismological environment, response spectrum, duration and cumulative energy, the ECSC technique can be easily implemented in the GCIM framework to directly simulate suitable ground motions for performance-based earthquake design and analysis.

2. ENERGY-COMPATIBLE AND SPECTRUM-COMPATIBLE GROUND-MOTION SIMULATION AND MODIFICATION

2.1. Stochastic simulation of ground motions using wavelet packets

Artificial ground motions can be generated using many numerical methods. As one special form of spectral presentation, the WPT was recently used to simulate nonstationary ground motions by Yamamoto and Baker [30]. The method has also been recently extended for simulating spatially correlated ground motions by Huang and Wang [31, 32]. There are several salient features of the models: (i) Unlike the Gasparini–Vanmarcke model [19], these new stochastic models can effectively characterize both amplitude and frequency nonstationarity of ground motions. The nonstationarity of ground motions can greatly affect nonlinear structural responses [7, 11, 33]. (ii)

Model parameters have been empirically calibrated as functions of seismological variables such as earthquake magnitude, source-to-site distance and site conditions. Therefore, synthetic ground motions can be generated based on hazard-consistent scenarios and (iii) simulated motions from the stochastic model have similar median and variability for a variety of IMs, which are consistent with the IM-based ground-motion prediction models (GMPM) [34]. Therefore, the wavelet-packet based stochastic models can be used for simulating future earthquakes.

The WPT is an advanced time–frequency analysis tool that decomposes a ground-motion time series $x(t)$ into a set of wavelet packets localized in the time (t) and frequency (f) domain. Specifically, for a time series $x(t)$, the wavelet packet coefficients $c_{j,k}^i$ are defined as:

$$c_{j,k}^i = \int_0^\infty x(t) \psi_{j,k}^i(t) dt \tag{1}$$

where $\psi_{j,k}^i(t)$ is the wavelet packet basis function, which is chosen as the Meyer wavelet function throughout this study, due to its good orthogonal property for time/frequency domain decomposition.

Given an acceleration time history in Figure 1(a), the time and frequency distribution of the squared wavelet packet coefficients $|c_{j,k}^i|^2$ is the wavelet packet spectrum (WPS), as shown in Figure 1(b). In this example, the time series contains $2^N = 4096$ ($N = 12$) data points evenly separated by a time interval $\Delta t = 0.01$ s. The subscript j denotes the level of wavelet packet decomposition, which is chosen as $j = 8$ throughout the study. The level of decomposition determines the frequency- and time-domain resolution of the WPS. As shown in Figure 1(b), if the sampling frequency (F_s) of the time history is 100 Hz; Nyquist frequency is $F_s/2 = 50$ Hz. Therefore, the wavelet-packet transform divides the frequency from 0 to the Nyquist frequency into bands of width $\Delta f_w = F_s/2^{j+1} = 0.1953$ Hz. In other words, the frequency axis is linearly discretized into 256 rows between 0 and 50 Hz. On the other hand, the time interval between the centers of adjacent wavelet packets $\Delta t_w = 2^j \cdot \Delta t = 2.56$ s.

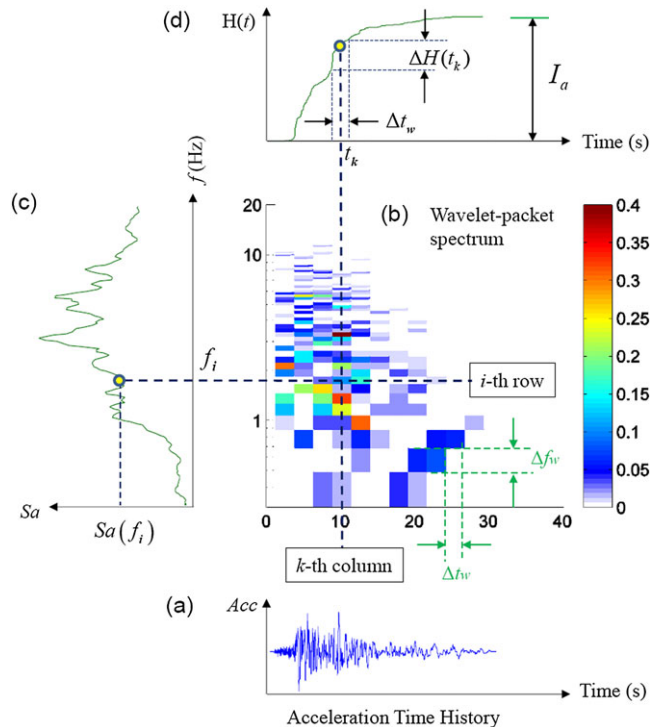


Figure 1. Wavelet packet spectrum, showing the distribution of squared wavelet packet coefficients of the recorded acceleration time history at the San Valley—Roscoe Blvd station in the 1994 Northridge earthquake. [Colour figure can be viewed at wileyonlinelibrary.com]

Therefore, the WPS is divided into $2^{N-j} = 16$ columns. Specifically, the notation $c_{j,k}^i$ denotes wavelet packet coefficient localized in the i -th row and the k -th column of the WPS.

Using inverse transformation, time series $x(t)$ can be precisely reconstructed via summation of wavelet packets over all rows ($i = 1$ to 2^j) and columns ($k = 1$ to 2^{N-j}):

$$x(t) = \sum_{i=1}^{2^j} \sum_{k=1}^{2^{N-j}} c_{j,k}^i \psi_{j,k}^i(t). \quad (2)$$

Additionally, the build-up of Ia with time is known as Husid function, defined as

$$H(t) = \frac{\pi}{2g} \int_{-\infty}^t |x(t)|^2 dt. \quad (3)$$

The Ia is related to Husid function when the above integration is made for the entire time history. On the other hand, it also equals to summation of all the squared coefficients in the WPS via Equation (4),

$$I_a = \frac{\pi}{2g} \int_0^\infty |x(t)|^2 dt = \frac{\pi}{2g} \sum_i \sum_k |c_{j,k}^i|^2. \quad (4)$$

According to Yamamoto and Baker [30], 13 wavelet packet parameters have been developed to fully characterize the statistical properties of the WPS, representing total energy, time- and frequency-domain distribution and correlation of the wavelet packet coefficients as summarized in Table I. One may consult Yamamoto and Baker [30], Huang and Wang [31, 32] for detailed information on the definition of wavelet packet parameters. It should be noted that some of the wavelet packet parameters are closely related to ground motion IMs. For example, the sum of squared wavelet packet coefficients, termed as E_{acc} , represents the total wave energy. It is also directly related to the Ia [35] by a constant factor $2g/\pi$ as shown in Equation (4). The functional form to predict these wavelet packet parameters using seismological variables has been also provided in [30],

$$Y(M_w, R_{hyp}, R_{rup}, V_{s30}) = \alpha + \beta_1 M_w + \beta_2 \ln(M_w) + \beta_3 \exp(M_w) + \beta_4 (R_{hyp} - R_{rup}) + \beta_5 \ln \sqrt{R_{rup}^2 + h^2} + \beta_6 \ln(V_{s30}) + \eta + \delta \quad (5)$$

where Y represents the natural logarithm of a wavelet packet parameter (except for the transformed correlation coefficient ρ); M_w is the moment magnitude, R_{rup} is the rupture distance, R_{hyp} is the hypocentral distance and V_{s30} is the average shear-wave velocity in the top 30 m. The parameter h denotes a fictitious depth in km. η and δ are intra- and inter-event residuals, respectively [30]. Given an earthquake scenario, the prediction model can be used to generate ground-motion time histories. Yamamoto [34] demonstrated that ground motions produced using the wavelet-packet simulation have a variety of IMs consistent in both predicted median and variation to existing prediction model in a wide range of magnitude, distance and site conditions. To model natural variability of ground motions, residuals of the model prediction are also analyzed, including the inter-event standard

Table I. Summary of wavelet parameters and parameter groups.

Energy parameters	Time-domain mean and standard deviation	Frequency-domain mean and standard deviation	Time-frequency correlation	Randomness parameter
E_{acc}	$E(t)_{major}$	$E(f)_{major}$	$\rho(t,f)_{major}$	$S(\xi)$
$E(a)_{major}$	$E(t)_{minor}$	$E(f)_{minor}$	$\rho(t,f)_{minor}$	
	$S(t)_{major}$	$S(f)_{major}$		
	$S(t)_{minor}$	$S(f)_{minor}$		

deviation and the intra-event standard deviation [30, 34]. Spatial correlation model of these residuals was also proposed for simulating spatially correlated ground motions [31, 32].

2.2. Energy-compatible and spectrum-compatible ground-motion simulation and modification algorithm

Orthogonal property of the WPS allows for independent modification of time and frequency characteristics of ground motions by adjusting wavelet packet coefficients. The wavelet packet coefficients $c_{j,k}^i$ of the initial motion $x(t)$ can be adjusted in the time and frequency domains iteratively to match a target response spectrum and build-up of wave energy with time, respectively. It is postulated that matching the build-up of Ia with time provides a critical constraint that can be used to better regulate the ‘ill-posed’ spectrum-matching problem and results in more realistic earthquake ground-motion time histories. The step-by-step algorithm of ECSC simulation/modification method is illustrated as follows, as is also shown in Figure 2. In this algorithm, ground motions are simulated and iteratively modified to match the target spectral acceleration and Husid function.

2.2.1. Simulation of a seed motion. Knowing earthquake scenario parameters (M_w, R, V_{s30}) , a target response spectrum $Sa^{target}(f)$, a target Husid function $H^{target}(t)$ and a seed ground-motion time history can be simulated using the following procedure.

First, the median wavelet-packet parameters $\bar{Y}(M_w, R_{hyp}, R_{rup}, V_{s30})$ are predicted using Equation (5) given these earthquake scenario parameters. Knowing the target Ia value from the target Husid function, several wavelet-packet parameters can be further improved. For example, the wavelet-packet parameter E_{acc} is directly related to the target Ia via $E_{acc} = \sum_i \sum_k |c_{j,k}^i|^2 = \frac{2g}{\pi} I_a^{target}$, and the target value is assigned to the seed motion. An epsilon is used to measure the number of standard deviation of the assigned E_{acc} value from the predicted median \bar{E}_{acc} via the following equation:

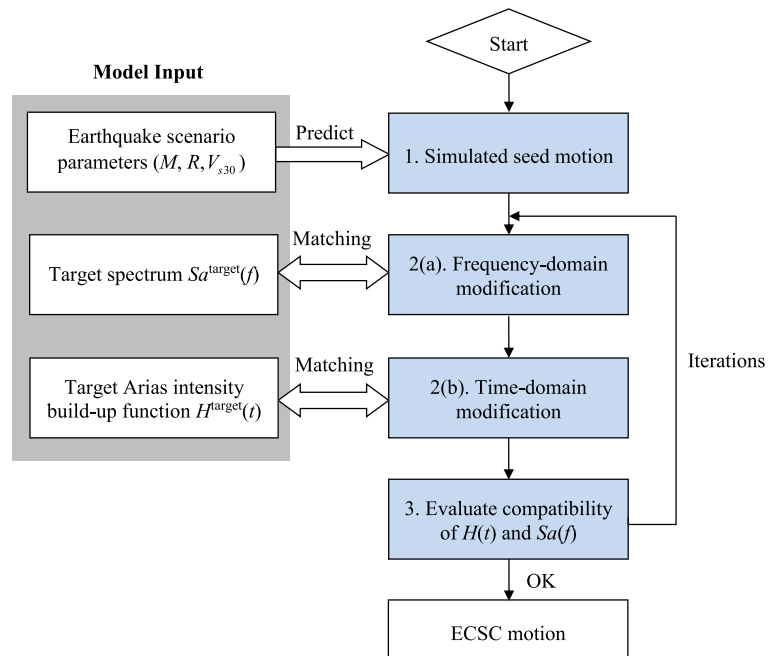


Figure 2. Illustration of the energy-compatible and spectrum-compatible (ECSC) simulation/modification algorithms. [Colour figure can be viewed at wileyonlinelibrary.com]

$$\varepsilon = (\ln E_{acc} - \ln \overline{E_{acc}}) / \sigma_{\ln E_{acc}} \quad (6)$$

where $\sigma_{\ln E_{acc}}$ (=0.85) is the standard deviation of E_{acc} in log scale. Because $E(a)_{\text{major}}$ is another energy parameter closely correlated with E_{acc} , its value can be determined following the conditional mean prediction:

$$\ln E(a)_{\text{major}} = \ln \overline{E(a)_{\text{major}}} + \varepsilon \cdot \rho_{\ln E_{acc}, \ln E(a)_{\text{major}}} \cdot \sigma_{\ln E(a)_{\text{major}}} \quad (7)$$

where $\rho_{\ln E_{acc}, \ln E(a)_{\text{major}}}$ is the correlation coefficient between E_{acc} and $E(a)_{\text{major}}$ in log scale, which is taken as 0.89 according to [34]. $\sigma_{\ln E(a)_{\text{major}}}$ (=1.13) is the standard deviation of $E(a)_{\text{major}}$ in log scale.

Given the predicted and updated wavelet-packet parameters, the initial seed motion $x(t)$ is then generated using inverse wavelet-packet transform following Equation (2).

2.2.2. Adjustment on the wavelet packet spectrum. The seed motion $x(t)$ is then modified to match the target spectrum and target Husid function by multiplying the wavelet packet coefficients of the seed motion using a weight matrix $w(i, k)$. The modified motion can be written as $y(t) =$

$\sum_{i=1}^{2^j} \sum_{k=1}^{2^{N-j}} w(i, k) c_{j,k}^i \psi_{j,k}^i(t)$, where $w(i, k)$ is the multiplier of wavelet packet coefficients $c_{j,k}^i$ localized around $f_i = i\Delta f_w$, $t_k = k\Delta t_w$, i.e., the center of the i -th row and j -th column of the WPS. The adjustment can be realized using a simple procedure to minimize the mismatch of spectrum and energy build-up iteratively.

(a) Frequency-domain modification to match acceleration response spectrum

Using superscript (n) to denote quantities of the n^{th} iteration, the simulated ground motion can be written as $y^{(n)}(t) = \sum_{i=1}^{2^j} \sum_{k=1}^{2^{N-j}} c_{j,k}^{i(n)} \psi_{j,k}^i(t)$. The weight of the WPS coefficients for the $(n + 1)^{\text{th}}$ iteration can be determined according to the ratio of target spectral acceleration $Sa^{\text{target}}(f_i)$ to simulated spectral acceleration $Sa(y^{(n)}(t), f_i)$ at oscillator frequency f_i via Equation (8):

$$w^{(n+1)}(i, \tilde{k}) = \frac{Sa^{\text{target}}(f_i)}{Sa(y^{(n)}(t), f_i)} \text{ for row } i \text{ and column } \tilde{k}. \quad (8)$$

Note the above modification is applied only to a specific WPS column number \tilde{k} for each frequency row i . Specifically, we first compute the instance $t_{\tilde{k}}$ corresponding to the peak acceleration of a 5% damped single-degree-of-freedom (SDOF) oscillator with natural frequency f_i under ground motion $y^{(n)}(t)$. This can be done during the process of calculating the response spectrum. Then, we find the WPS column \tilde{k} in which $t_{\tilde{k}}$ is contained, i.e. $(\tilde{k} - 1)\Delta t_w < t_{\tilde{k}} \leq \tilde{k}\Delta t_w$.

Because each row in the wavelet-packet spectrum covers a range of frequencies bounded by $(\frac{(i-1)F_s}{2^{j+1}}, \frac{iF_s}{2^{j+1}})$, where $i = 1, 2, \dots, 2^j$, $F_s = 100$, $j = 8$, modification of a wavelet packet in a row could affect a range of frequencies. In this study, we match the spectral acceleration only at a single frequency ($f_i = \frac{iF_s}{2^{j+1}}$) in each row modification. Therefore, the modification process has fixed frequency resolution, which is different relative to some of the competing spectral matching algorithms [19, 37].

It is also worth pointing out that the frequency-domain modification changes response spectra differently in different frequency ranges. A recent study [36] showed that scaling of response spectral ordinates in the low to middle oscillator-frequency can be treated as being equivalent to the scaling of the corresponding frequency in Fourier spectrum. However, the PGA and spectral ordinates at high oscillator-frequencies ($f \geq 20$ Hz) are controlled by the entire frequency band instead of the high-frequency component of the ground motion. In this study, the PGA of the

simulated motion is adjusted directly to match the target PGA. The lowest and the highest frequency for the row modification is set as 0.195 and 20 Hz, respectively (e.g. $f_1=0.195, f_2=0.391, f_3=0.586, \dots, f_{102}=19.922\text{Hz}$). After the frequency-domain modification, the modified motion is written as

$$y^{(n+1)}(t) = \sum_{i=1}^{2^j} \sum_{k=1}^{2^{N-j}} w^{(n+1)} c_{j,k}^{i(n)} \psi_{j,k}^i(t) = \sum_{i=1}^{2^j} \sum_{k=1}^{2^{N-j}} c_{j,k}^{i(n+1)} \psi_{j,k}^i(t).$$

(b) Time-domain modification to match Ia build-up

To match the Ia build-up process, the increment of Husid function of the target and simulated motions should match within each WPS time interval. Accordingly, a piece-wise weighting function can be determined to modulate the amplitude of the acceleration time history in each time interval via Equation (9):

$$w^{(n+2)}(t) = \sqrt{\frac{\Delta H^{\text{target}}(t_k)}{\Delta H^{(n+1)}(t_k)}} \text{ for all column } k = 1, 2, \dots, 2^{N-j} \text{ and } t \in [t_{k-1}, t_k] \quad (9)$$

where $\Delta H(t_k) = H(t_k) - H(t_{k-1})$ is the increment of the Husid function over the WPS time interval $[t_{k-1}, t_k]$, and $t_k = k\Delta t_w$. Of course, the weighting function can also be smoothed in practical use. After the time-domain modification, The modified motion then can be written as $y^{(n+2)}(t) = w^{(n+2)}(t) \times y^{(n+1)}(t)$.

2.2.3. *Evaluating compatibility of $H(t)$ and $Sa(f)$.* To measure the compatibility of spectral acceleration and Ia build-up, the following mean squared errors (MSEs) are defined to quantify the relative difference in Sa and $H(t)$ between the simulation and the target. Because $H(t)$ is an accumulative function, it is more sensible to compare the increments instead of the absolute values.

$$\text{MSE}_{Sa} = \frac{1}{n} \sum_{i=1}^n (\ln Sa(y(t), f_i) - \ln Sa^{\text{target}}(f_i))^2 \quad (10)$$

$$\text{MSE}_{H(t)} = \frac{1}{m} \sum_{k=1}^m \left(\frac{\Delta H^{\text{target}}(t_k)}{\Delta H(y(t), t_k)} - 1 \right)^2 \quad (11)$$

Steps 2.2.2(a) and 2.2.2(b) will be iterated until the MSEs in Sa and $H(t)$ reach a desired level. In the end, baseline correction on the modified accelerogram will be performed to eliminate permanent drifts in the ground velocity and displacement time histories.

It is worth mentioning that the proposed approach is different from many existing spectral matching approaches that adjust ground-motion time histories either in the frequency domain [38] or in the time domain [37, 39, 40]. Although the time-domain approach can result in a modified motion that preserves the normalized Ia build-up process of the seed motion, it has been reported that the procedure cannot control the value of Ia itself [41]. The method is only suitable for slight modification of the spectral shape and relies heavily on the sensible choice of seed motions.

2.3. An illustrative example

In this section, an illustrative example of the ECSC method is presented using the ground motion recorded at the El Centro Array #10 station in the 1979 Imperial Valley earthquake as a target motion. Figure 3(a) shows the target acceleration time history, its WPS, 5%-damped acceleration response spectrum and Ia build-up. Among them only response spectrum and Ia build-up are used as targets in the ECSC modification process, while its acceleration time history and WPS are only illustrated for reference. As discussed in section 2.2.1, a seed motion $x(t)$ is first stochastically simulated using seismological parameters of the target motion ($M_w = 6.53, R_{rup} = 6.17 \text{ km}, R_{hyp} = 28.13 \text{ km}, V_{s30} = 203 \text{ m/s}$), as shown in Figure 3(b). It can be observed that neither spectral accelerations nor $H(t)$ can match those of the target motion, except that Ia of the seed motion matches the target value as it is directly assigned. Mean squared errors of Sa and $H(t)$ between the seed motion and the target

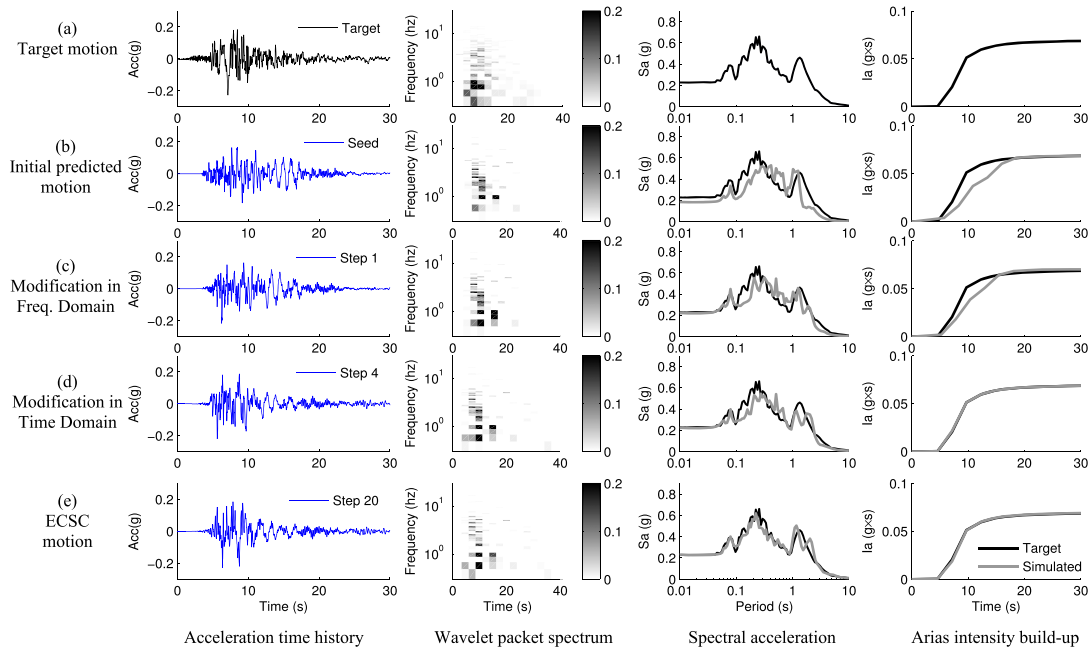


Figure 3. ECSC simulated ground motions, wavelet packet spectrum, response spectra and the build-up of Arias intensity compared with the recorded motion at the El Centro Array #10 station in the 1979 Imperial Valley earthquake.

are plotted in Figure 4, denoted as the 0th step. Subsequently, Figure 3(c) shows the simulated motion after the 1st step frequency-domain modification, which reduces MSEs of Sa and $H(t)$ as shown in Figure 4. Then, the 2nd step, time-domain modification, is performed to match Ia build-up following the procedure described section 2.2.2(b). Again, the 3rd step is frequency-domain modification and the 4th step is time-domain modification. Figure 3(d) shows after the step 4, Husid function of the simulated motion closely matches the target, although the spectrum compatibility needs further improvement. The convergence profile in Figure 4 clearly demonstrated that the MSEs in Sa and $H(t)$ will not reduce further after 20 iterations. The ‘converged’ motion is termed as the ECSC simulated ground motion, as shown in Figure 3(e).

In general, convergence of MSEs of Sa and $H(t)$ is not strictly monotonic. Many of our tests showed that MSEs become relatively stable after 20 iterations. It is desirable to get converged MSEs below 0.02. Otherwise, it is advised to use a different seed to perform the ECSC simulation/modification again.

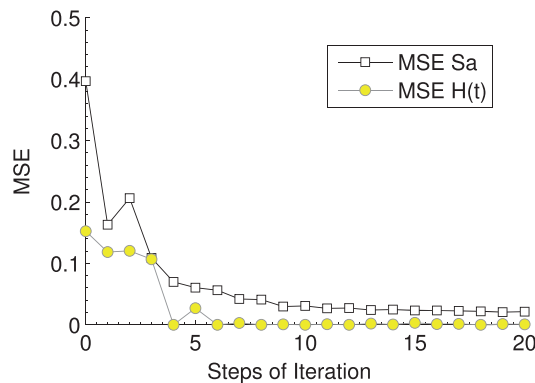


Figure 4. Convergence of Sa and $H(t)$ in iterations.

By visual inspection, the ECSC simulated ground motion closely matches the response spectrum and Ia build-up of the recorded motion. Apparently, they also have very similar peak ground accelerations (PGAs) (around 0.23 g) and durations. Furthermore, change in time-domain and frequency-domain characteristics of ground motions can be better represented in modification of WPS in Figure 3. The wavelet packet coefficients of the seed motion appear to be larger and densely populated at around 0.8 Hz, which may explain its higher spectral accelerations in that frequency range. Frequency- and time-domain modification changed the amplitude and distribution of wavelet packet coefficients. After iterations, WPS of the ECSC simulated motion shares a high degree of overall similarity with that of the target motion in terms of amplitude and distribution.

It should be also noted that the generation of the initial seed motion $x(t)$ in Step 0 is still a random process, as described by Huang and Wang [31, 32]. Random realization of wavelet-packet parameters will result in different seed motions using the same seismological variables. Figure 5 shows five representative ECSC simulated ground motions, labeled as ‘Sim 1’ to ‘Sim 5’, generated from different seed motions. By visual inspection, waveforms of the five simulations are similar to that of the actual recorded motion in terms of acceleration, velocity and displacement time histories, even though these time histories are not used as target in the simulation/modification process. It is interesting to notice that all simulations generate a velocity pulse with a peak value greater than 40 cm/s at around 8 s, similar to that of the recorded motion. Moreover, the peak ground displacements (PGDs) of three simulations are above 20 cm, similar to that of the recorded motion.

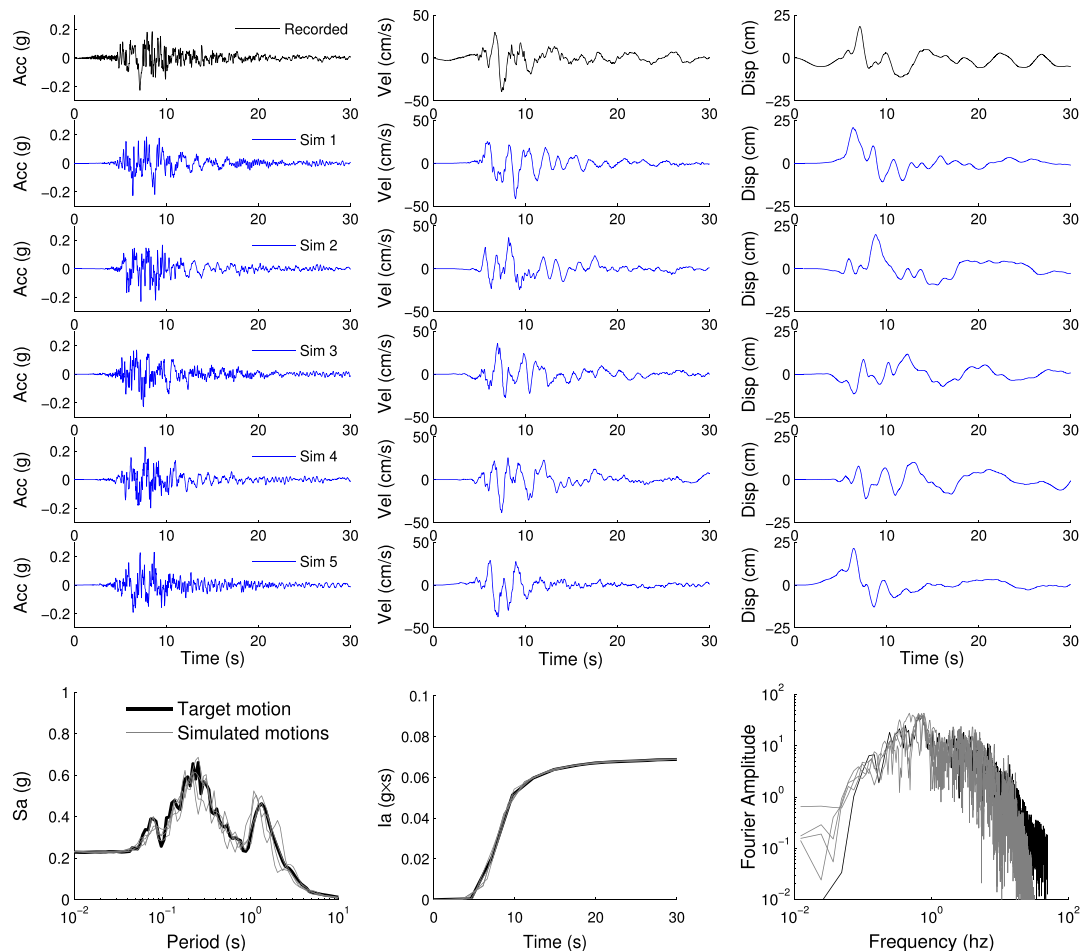


Figure 5. Five realizations of ECSC simulated ground motions, their response spectra and build-up of Ia compared with ground motion recorded at the El Centro Array #10 station in the 1979 Imperial Valley earthquake.

Figure 5 also shows comparison of response spectra, build-up of Ia and the Fourier spectra. In general, all five simulated motions captured the frequency content and energy content of the recorded motion reasonably well.

3. ENERGY-COMPATIBLE AND SPECTRUM-COMPATIBLE SIMULATED GROUND MOTION DATASET

The proposed ECSC simulation technique provides a viable approach to generate synthetic ground motions that match both response spectra and energy build-up process with actual recorded motions. The method can be used to ‘reproduce’ recorded ground motions to form a large dataset. Performance of the ECSC method can be quantified by one-to-one comparison of several important ground motion *IMs* between the recorded and simulated ground-motion datasets. Specifically, six *IMs* are examined in this section including the PGA, peak ground velocity (PGV), PGD, significant duration (D_{5-95}), Ia and cumulative absolute velocity (CAV [42]).

3.1. Strong-motion dataset

A total of 562 ground-motion records from three large earthquakes in California are selected in the validation test. They are the 1979 Imperial Valley earthquake, the 1989 Loma Prieta earthquake and the 1994 Northridge earthquake. Table II provides information of these three events. Ground motions are recorded in both strike-normal and strike-parallel directions (281 pairs) and are retrieved from the Pacific Earthquake Engineering Research Center (PEER) Next Generation Attenuation (NGA) strong-motion database. Figure 6 shows locations of seismograph stations and epicenters of the three events. Using the ECSC method, each actual recorded motion is stochastically simulated using seismological variables (M , R , V_{s30}) associated with that record. In this way, all 562 waveforms are ‘reproduced’ and referred to as the ECSC simulated dataset.

Figure 7 presents six representative recordings (in black line) from the NGA database and their counterparts (in blue line) from the ECSC dataset. The target ground motions include records at (a) the H-E13 and (b) the H-E04 station during the Imperial Valley earthquake, ground motions recorded at (c) the Bear Valley and (d) the Foster City station during the Loma Prieta earthquake, and ground motions recorded at (e) the Griffith Park and (f) the Sylmar station during the Northridge earthquake. The rupture distance of these stations ranges from 5 to 52 km, while the recorded PGA ranges from 0.12 to 0.68 g. Side-by-side comparisons of the actual recorded and

Table II. Earthquake events used to generate energy-compatible and spectrum-compatible (ECSC) dataset

Event	Date (yyyy/mm/dd)	Moment Magnitude	Location	Number of recordings
Imperial Valley	1979/10/15	6.53	California	49
Loma Prieta	1989/10/18	6.93	California	82
Northridge	1994/01/17	6.69	California	150

simulated acceleration time histories, velocity time histories and displacement time histories are provided. By visual inspection, the simulated and recorded acceleration time histories are found to be similar in terms of both time and frequency characteristics. Response spectra and Ia build-up for each pair of recorded and simulated ground motions are also compared in Figure 7. Both of them match very well.

3.2. Comparison of ground-motion intensity measures

Ground motions in the ECSC dataset and their recorded counterparts in the NGA dataset are compared in terms of seven important ground-motion *IMs*, including PGA, PGV, PGD, Ia, CAV and D_{5-95} . The

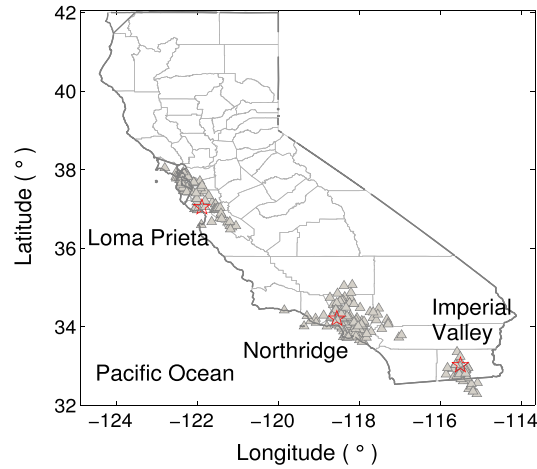


Figure 6. Epicenters (stars) and locations of earthquake recording stations (triangles) used in this study.

residual term $r_{\ln IM}$ is defined to quantify the relative difference between IMs (in the natural log scale) using Equation (12):

$$r_{\ln IM} = \ln(IM_{NGA}) - \ln(IM_{ECSC}). \quad (12)$$

Mean and standard deviation of $r_{\ln IM}$ are summarized in Figure 8(a). On average, the mean of $r_{\ln IM}$ is in the range of 0 to 0.05 for PGA, PGV, D_{5-95} , Ia and CAV, while the standard deviation is in the range of 0 to 0.1. The results show that the ECSC simulation is overall unbiased to reproduce these IMs. Majority of simulated IMs only deviate from the recorded motion by much less than 10%. On the other hand, the mean and standard deviation of PGD residuals are 0.21 and 0.46, respectively. It indicates that, on average, the PGDs of the ECSC ground motions are smaller than the recorded counterparts by 23%, and variation is much larger than other IMs. On the other hand, the relative difference between spectral accelerations can be quantified using:

$$r_{\ln Sa} = \ln(Sa(T)_{NGA}) - \ln(Sa(T)_{ECSC}). \quad (13)$$

Figure 8(b) shows the mean and standard deviation of $r_{\ln Sa(T)}$ for $T = 0.01$ to 5 s. It is observed that the mean of residuals is in the range of -0.15 to 0.15 . The standard deviation of residuals increases with period, from less than 0.2 in the short periods (i.e. 0–0.5 s) to around 0.5 in the long period (5 s). The results indicate the ECSC method cannot obtain the same accuracy in simulating the long period characteristics of ground motions as it does for the short period.

4. TIME HISTORY ANALYSES OF ELASTO-PLASTIC OSCILLATORS USING ECSC AND NGA DATASETS

4.1. Single-degree-of-freedom (SDOF) elasto-plastic oscillator

Nonlinear hysteretic analyses are often used to estimate lateral displacement and base shear demand of structures under earthquake loading. In this section, we conduct one-to-one comparison of the dynamic response of SDOF elasto-plastic oscillators using the simulated and the recorded ground motions. Figure 9(a) shows the force–displacement relationship of a bilinear elasto-plastic oscillator with post-yield stiffness equals 5% of the elastic stiffness. As shown in Figure 9(b), the oscillator is designed according to the design response spectrum of site class C ($S_s = 1.5$ g, $S_l = 0.6$ g, $F_a = 1.0$, $F_v = 1.3$) recommended by National Earthquake Hazards Reduction Program (NEHRP) [43]. If the oscillator has an elastic fundamental period T_0 , its yield displacement D_y can be computed as:

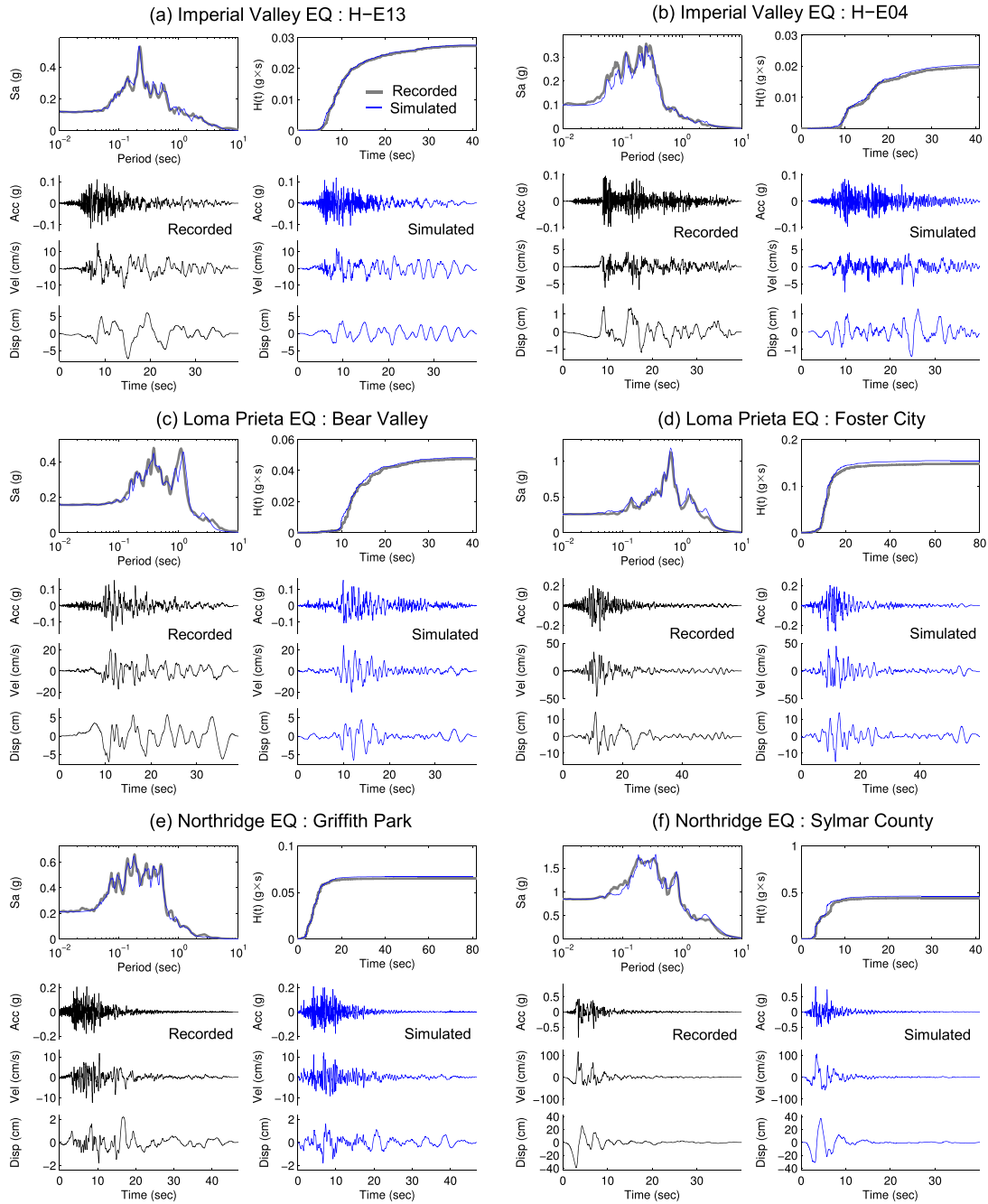


Figure 7. Comparison of time histories, response spectra and Arias intensity build-up for six selected stations from the NGA recorded dataset and the ECSC simulated dataset.

$$D_y = Sa(T_0)(T_0/2\pi)^2/R \quad (14)$$

where R is the strength reduction factor that shows the level of ductility demands of the oscillator model. Note that the term $Sa(T_0)(T_0/2\pi)^2$ in Equation (12) equals to the spectral displacement, which is defined as the maximum relative displacement of an elastic oscillator. For example, if $T_0 = 1$ s, $R = 1$, the yield displacement D_y is computed as 19.4 cm, which equals to the maximum displacement of an elastic oscillator. In other words, the elasto-plastic oscillator remains in the linear

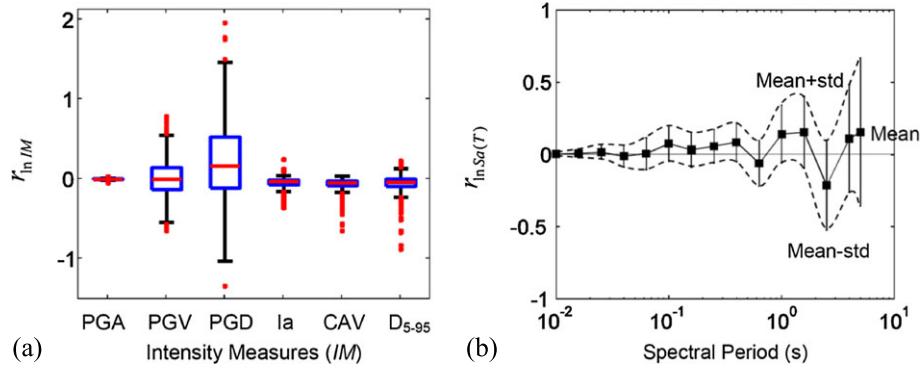


Figure 8. Comparison of NGA and ECSC dataset. (a) Box plot of residuals of PGA, PGV, PGD, Ia, CAV and D_{5-95} and (b) mean and mean \pm std of spectral acceleration residuals.

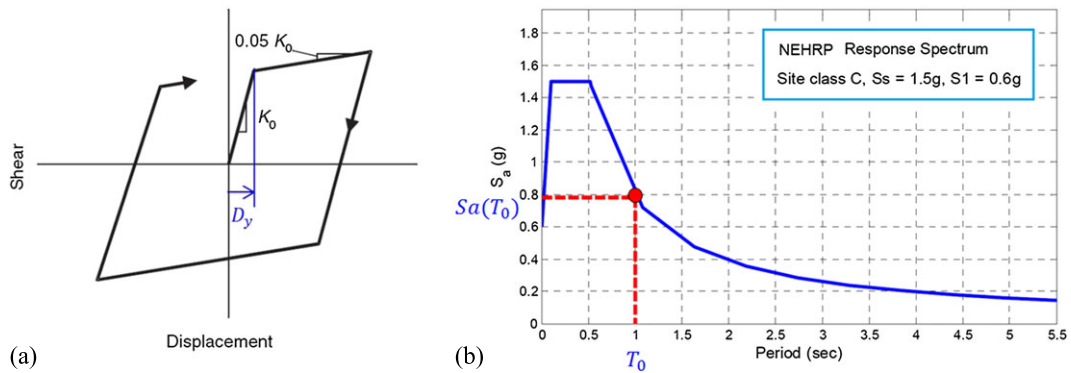


Figure 9. (a) Illustration of force–displacement relationship for a single-degree-of-freedom (SDOF) elastoplastic hysteretic system, and (b) NEHRP 5%-damped design response spectrum for Site Class C.

range. Increasing R reduces the yield displacement and drives the oscillator model into nonlinear range. In this study, a total of 48 SDOF oscillators with a combination of eight strength reduction factor R (i.e., 1, 2, 3 ... 8) and six fundamental periods (i.e., 0.1, 0.2, 0.5, 1, 2, 5 s) are used.

4.2. Comparison of oscillator responses under the ECSC simulated and the recorded motions

Although the ECSC simulated motions resemble the recorded motions in terms of response spectrum and accumulative energy, their capability to produce similar nonlinear oscillator responses should be tested. Time-history analyses of the oscillators are conducted using a total of 562 recorded motions and the same number of ECSC counterparts generated in Section 3.1. In time history analyses, ground motion amplitudes are scaled to match the design spectrum at the oscillator-period T_0 through a scaling factor f , which can be easily determined as $f = \frac{Sa_{design}(T_0)}{Sa(T_0)}$. The scaled motions are intensive to drive the oscillators into the nonlinear range when $R > 1$.

The maximum relative displacement and the absolute peak acceleration of the oscillators are recorded for one-to-one comparison. Residuals r_{InDisp} and r_{InAcc} are defined to quantify the difference in the maximum relative displacement and the absolute peak acceleration as follows,

$$r_{InDisp} = \ln(\text{Disp}_{NGA}) - \ln(\text{Disp}_{ECSC}) \quad (15)$$

$$r_{InAcc} = \ln(\text{Acc}_{NGA}) - \ln(\text{Acc}_{ECSC}) \quad (16)$$

where subscript ‘NGA’ denotes that the oscillator response is calculated using a recorded motion from the NGA database, while ‘ECSC’ denotes the response is from its ECSC simulated counterpart.

Figure 10 shows the mean and standard deviation of the displacement residuals versus strength reduction factors. On average, the mean of displacement residuals is well bounded within ± 0.1 . The standard deviation of residuals increases sharply from 0.05 to around 0.35, when R increases from 1 to 8. On the other hand, the mean and standard deviation of acceleration residuals are less than that of the displacement residuals. Figure 11 shows that the mean of acceleration residuals is well bounded within ± 0.05 , while the standard deviation gradually increases from 0.02 to around 0.2, when R increases from 1 to 8. The above numerical analyses clearly demonstrate that the ECSC ground motions can result in overall unbiased prediction of seismic responses of nonlinear oscillators. The performance of the ECSC ground motions would not deteriorate significantly even when highly nonlinear systems are involved.

5. APPLICATION OF ECSC SIMULATION IN GCIM FRAMEWORK

5.1. The generalized conditional intensity measure (GCIM) framework

As demonstrated in the previous sections, the ECSC simulation provides a viable approach to simulate ground-motion time histories that match multiple target IMs. Obviously, matching the Ia build-up process, a.k.a. the Husid function $H(t)$, also implies the matching of several ground-motion duration

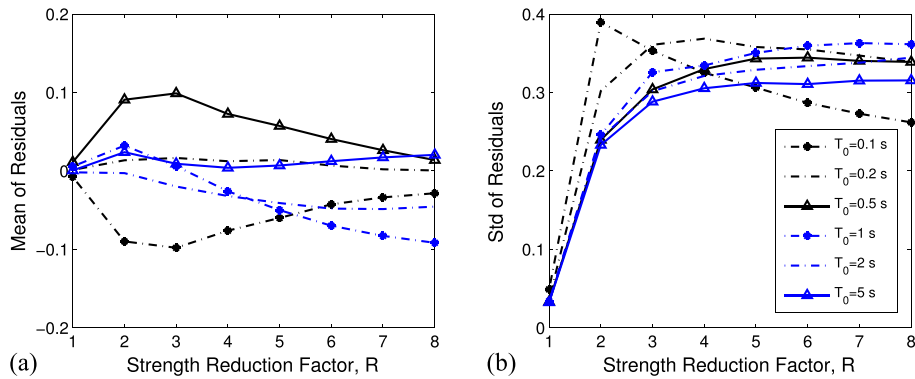


Figure 10. (a) Mean and (b) standard deviation of residuals for the maximum response displacements calculated using scaled ground-motion datasets versus different strength reduction factors (R) and oscillator periods (T_0).

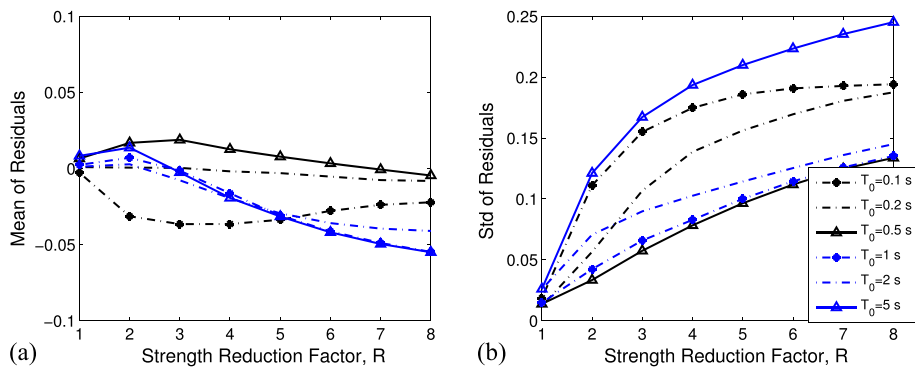


Figure 11. (a) Mean and (b) standard deviation of residuals for the maximum response acceleration calculated using scaled ground-motion datasets versus different strength reduction factors (R) and oscillator periods (T_0).

measures, such as D_{5-75} and D_{5-95} . Therefore, the ECSC method can be easily implemented in the GCIM framework to generate suitable ground motions for performance-based earthquake design and analysis. Different from the previous GCIM studies, the ground motions will be directly simulated instead of being selected from a database.

Given an earthquake scenario, statistical distribution of the spectral accelerations, significant durations (D_{5-75} , D_{5-95}) and I_a can be determined following the GCIM procedure [24–26]. Key to this procedure, empirical cross-correlations between these IMs [e.g. [44–47]] need to be preserved through multivariate random realizations. Figure 12(a) shows 60 randomly realized spectral accelerations for an earthquake scenario ($M_w = 7$, $R_{rup} = 10$ km, strike-slip faulting) conditioned on $T = 1$ s with $\epsilon = 0$, following the GCIM procedure. Correspondingly, the cumulative distribution functions (CDFs) of significant duration parameters, D_{5-75} , D_{5-95} and I_a are shown in Figure 12(b) for this scenario. In Figure 12, we also highlight a single realization of the spectral acceleration and its corresponding values of significant durations (D_{5-75} , D_{5-95}) and I_a , which are determined as 6.7 s, 12.5 s and 1.2 m/s, respectively. These values will be used to construct the target Husid function for the ECSC simulation in the next section.

5.2. The target Husid function and ECSC simulation

According to [48], the normalized Husid function, as shown in Figure 13, can be well approximated by a lognormal CDF via the following function:

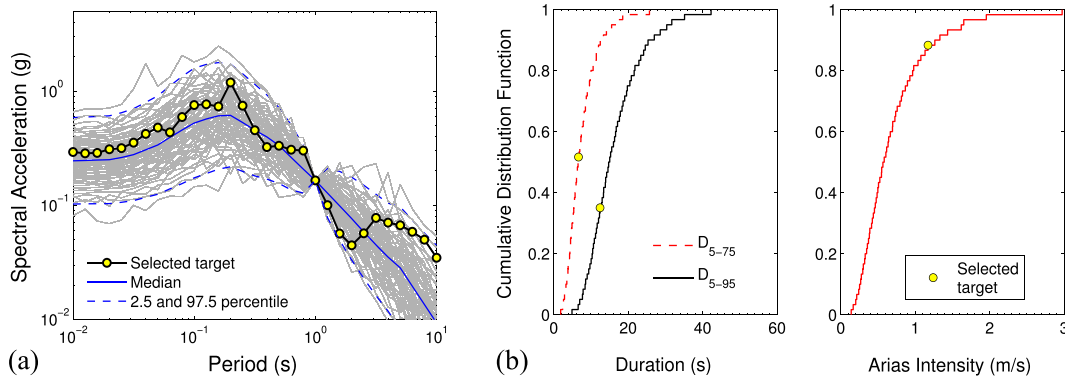


Figure 12. (a) Distribution of spectral accelerations following the generalized conditional intensity measure (GCIM) framework and a selected target S_a . (b) Cumulative distribution functions (CDFs) of D_{5-75} , D_{5-95} and Arias intensity. The open circles represent corresponding values of the selected targets.

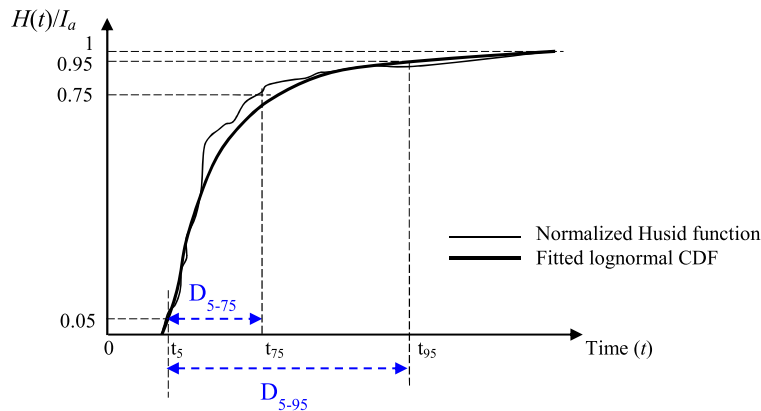


Figure 13. Normalized Husid function and fitted lognormal CDF.

$$H(t) = \Phi\left(\frac{\ln(t) - \mu}{\sigma}\right) \times I_a \quad (17)$$

where Φ is the CDF of the standard normal distribution, μ and σ are two parameters to be determined, which can be solved analytically if D_{5-75} and D_{5-95} are given. Define t_5 , t_{75} and t_{95} as the time instances when 5, 75 and 95% of normalized Husid function are accumulated, which can be written as:

$$\begin{cases} t_5 = \exp(\mu) \times \exp(\sigma \cdot \Phi^{-1}(0.05)) \\ t_{75} = \exp(\mu) \times \exp(\sigma \cdot \Phi^{-1}(0.75)) \\ t_{95} = \exp(\mu) \times \exp(\sigma \cdot \Phi^{-1}(0.95)) \end{cases} \quad (18)$$

Therefore, D_{5-75} and D_{5-95} can be computed as follows:

$$\begin{cases} D_{5-75} = t_{75} - t_5 = \exp(\mu) \cdot [\exp(\sigma \cdot \Phi^{-1}(0.75)) - \exp(\sigma \cdot \Phi^{-1}(0.05))] \\ D_{5-95} = t_{95} - t_5 = \exp(\mu) \cdot [\exp(\sigma \cdot \Phi^{-1}(0.95)) - \exp(\sigma \cdot \Phi^{-1}(0.05))] \end{cases} \quad (19)$$

Given the ratio of D_{5-75} and D_{5-95} , σ in $H(t)$ can be solved numerically via the following expression:

$$\frac{D_{5-95}}{D_{5-75}} = \frac{\exp(\sigma \cdot \Phi^{-1}(0.95)) - \exp(\sigma \cdot \Phi^{-1}(0.05))}{\exp(\sigma \cdot \Phi^{-1}(0.75)) - \exp(\sigma \cdot \Phi^{-1}(0.05))} \quad (20)$$

And μ in $H(t)$ can be solved by Equation (21):

$$\mu = \ln\left[\frac{D_{5-95}}{\exp(\sigma \cdot \Phi^{-1}(0.95)) - \exp(\sigma \cdot \Phi^{-1}(0.05))}\right] \quad (21)$$

The above procedure converts the target significant durations and I_a generated from GCIM to the target Husid function $H(t)$ for the subsequent ECSC simulation.

Figure 14 compares the S_a and $H(t)$ of an ECSC simulated ground motion with the targets highlighted in Figure 12. Clearly, both response spectrum and I_a build-up of the simulated motion

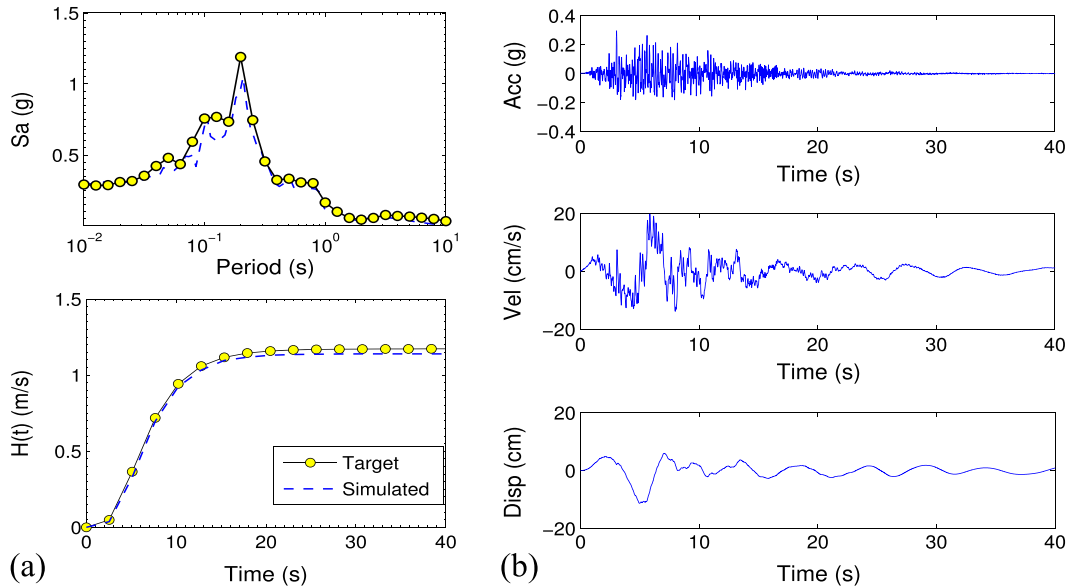


Figure 14. (a) Target and simulated spectral acceleration, Arias intensity build-up. (b) Acceleration, velocity and displacement time histories of the simulated ground motion.

agree well with the targets. Specifically, D_{5-75} , D_{5-95} and I_a of the simulated motion are reported to be 6.3 s, 11.8 s and 1.15 m/s respectively. Obviously, the simulation procedure can be repeated for other selected targets of S_a , D_{5-75} , D_{5-95} and I_a build-up such that a full set of simulated motions can be generated to follow the targeted distribution of these multiple IMs for a specific earthquake scenario. This example demonstrates the great potential for the ECSC method to be implemented in the GCIM framework.

6. CONCLUSIONS

In this study, a new ground-motion simulation and modification procedure was presented that allows the generation of ECSC ground motions through wavelet packet characterization and modification. The WPT has basis functions that are orthogonal and localized in time and frequency domains. The salient feature allows for ground-motion time histories to be flexibly adjusted in frequency domain and time domain simultaneously, thus, modifying their response spectrum and I_a build-up. The procedure is based on three key steps, starting from prediction of a seed motion using seismological constraints (M_w , R , V_{s30}), followed by iterative adjustments of the wavelet packet spectrum in both time and frequency domain and, finally, evaluating compatibility of response spectrum and I_a build-up of the simulated motion with targets.

The ECSC procedure was demonstrated by one-to-one comparison of several important IMs (e.g. PGA, PGV, PGD, I_a) between simulated ECSC ground motions and actual recorded NGA ground motions. Extensive numerical simulations were also performed to compare the nonlinear responses of elasto-plastic oscillators using the simulated ECSC ground motions and recorded motions. The tests validated that the general performance of the simulated ECSC ground motions are comparable with that of the recorded motions. More examples to validate the ECSC ground motions using other structural types or geotechnical systems can be found in Huang [49].

As the ECSC procedure can be regarded as stochastic ground-motion modeling conditioned on a given seismological environment, response spectrum, duration and I_a build-up, the ECSC technique can be easily implemented in the GCIM framework to directly simulate suitable ground motions for performance-based earthquake design and analysis. The simulation can be repeated for many realizations such that a collection of the simulated motions will follow the targeted distribution of spectral accelerations, duration and I_a for a specific earthquake scenario. Different from the previous GCIM studies, the ground motions are directly simulated instead of being selected from a database.

The ECSC simulation software can be accessed from the authors' website at http://ihome.ust.hk/~gwang/ECSC_simulation.html.

ACKNOWLEDGMENTS

The study was supported by the Hong Kong Research Grants Council (RGC) through the General Research Fund grant no 16213615 and University Grants Council (UGC) Research Infrastructure grant no. IRS16EG15. The authors would like to acknowledge Jack Baker for sharing the source code for ground-motion simulation at http://www.stanford.edu/~bakerjw/gm_simulation.html.

REFERENCES

1. Wang G. A ground motion selection and modification method capturing response spectrum characteristics and variability of scenario earthquakes. *Soil Dynamics and Earthquake Engineering* 2011, **31**:611–625.
2. Wang G, Youngs R, Power M, Li Z. Design ground motion library (DGML): an interactive tool for selecting earthquake ground motions. *Earthquake Spectra* 2015, **31**(2):617–635.
3. Vanmarcke EH, Heredia-Zavoni E, Fenton GA. Conditional simulation of spatially correlated earthquake ground motion. *Journal of Engineering Mechanics* 1993, **119**(11):2333–2352.
4. Conte JP, Peng BF. Fully nonstationary analytical earthquake ground-motion model. *Journal of Engineering Mechanics* 1997, **123**(1):15–24.
5. Atkinson G, Boore D. Stochastic point-source modeling of ground motions in the Cascadia region. *Seismological Research Letters* 1997, **68**:74–85.

6. Atkinson G, Silva W. Stochastic modeling of California ground motions. *Bulletin of the Seismological Society of America* 2000, **90**:255–274.
7. Spanos P, Giaralis A, Politis N. Time frequency representation of earthquake accelerograms and inelastic structural response records using the adaptive chirplet decomposition and empirical mode decomposition. *Soil Dynamics and Earthquake Engineering* 2007, **27**(7):675–689.
8. Rezaeian S, Kiureghian AD. A stochastic ground motion model with separable temporal and spectral nonstationarities. *Earthquake Engineering & Structural Dynamics* 2008, **37**:1565–1584.
9. Rezaeian S, Kiureghian AD. Simulation of synthetic ground motions for specified earthquake and site characteristics. *Earthquake Engineering & Structural Dynamics* 2010, **39**:1155–1180.
10. Zentner I. A procedure for simulating synthetic accelerograms compatible with correlated and conditional probabilistic response spectra. *Soil Dynamics and Earthquake Engineering* 2014, **63**:226–233.
11. Li Y, Conte J, Barbato M. Influence of time-varying frequency content in earthquake ground motions on seismic response of linear elastic systems. *Earthquake Engineering & Structural Dynamics* 2016; in press.
12. Pitarka A, Irikura K, Iwata T, Sekiguchi H. Three dimensional simulation of the near-fault ground motion for the 1995 Hyogo-ken Nanbu (Kobe), Japan, Earthquake. *Bulletin of the Seismological Society of America* 1998, **88**(2):428–440.
13. He CH, Wang JT, Zhang CH, Jin F. Simulation of broad band seismic ground motions at dam canyons by using a deterministic numerical approach. *Soil Dynamics and Earthquake Engineering* 2015, **76**:136–144.
14. Graves RW, Pitarka A. Broadband ground-motion simulation using a hybrid approach. *Bulletin of the Seismological Society of America* 2010, **100**(5A):2095–2123.
15. Shome N, Cornell CA, Bazzurro P, Carballo JE. Earthquakes, records, and nonlinear responses. *Earthquake Spectra* 1998, **14**(3):469–500.
16. Baker JW, Cornell CA. Spectral shape, epsilon and record selection. *Earthquake Engineering & Structural Dynamics* 2006, **35**(9):1077–1095.
17. Chopra AK. *Dynamics of Structures* (4th edn). Prentice Hall, 2011.
18. Jayaram N, Lin T, Baker JW. A computationally efficient ground-motion selection algorithm for matching a target response spectrum mean and variance. *Earthquake Spectra* 2011, **27**(3):797–815.
19. Gasparini DA, Vanmarcke EH. *Simulated Earthquake Motions Compatible with Prescribed Response Spectra*. Department of Civil Engineering: M.I.T, 1976.
20. Ostadan F, Mamoon S., Arango I. Effect of input motion characteristics on seismic ground response, *Eleventh World Conference on Earthquake Engineering*, Paper No. 1924., Acapulco, Mexico, June 23–28, 1996.
21. Chandramohan R, Baker JW, Deierlein GG. Impact of hazard-consistent ground motion duration in structural collapse risk assessment. *Earthquake Engineering & Structural Dynamics* 2016, **45**(8):1357–1379.
22. Chandramohan R, Baker JW, Deierlein GG. Quantifying the influence of ground motion duration on structural collapse capacity using spectrally equivalent records. *Earthquake Spectra* 2016, **32**(2):927–950.
23. Wang G. Efficiency of scalar and vector intensity measures for seismic slope displacements. *Frontiers of Structural and Civil Engineering* 2012, **6**(1):44–52.
24. Bradley BA. A generalized conditional intensity measure approach and holistic ground-motion selection. *Earthquake Engineering & Structural Dynamics* 2010, **39**(12):1321–1342.
25. Bradley BA. The seismic demand hazard and importance of the conditioning intensity measure. *Earthquake Engineering & Structural Dynamics* 2012, **41**:1417–1437.
26. Tarbali K, Bradley BA. Ground motion selection for scenario ruptures using the generalized conditional intensity measure (GCIM) method. *Earthquake Engineering & Structural Dynamics* 2015, **44**(1):601–1621.
27. Baker JW. Conditional mean spectrum: tool for ground motion selection. *Journal of Structural Engineering* 2011, **137**(3):322–331.
28. Kwong NS, Chopra AK. Evaluation of the exact conditional spectrum and generalized conditional intensity measure methods for ground motion selection. *Earthquake Engineering & Structural Dynamics* 2015; online.
29. Kwong NS, Chopra AK, McGuire RK. Evaluation of ground motion selection and modification procedures using synthetic ground motions. *Earthquake Engineering & Structural Dynamics* 2015, **44**(11):1841–1861.
30. Yamamoto Y, Baker JW. Stochastic model for earthquake ground motion using wavelet packets. *Bulletin of the Seismological Society of America* 2013, **103**(6):3044–3056.
31. Huang D, Wang G. Stochastic simulation of regionalized ground motions using spatial cross-correlation model and cokriging analysis. *Earthquake Engineering & Structural Dynamics* 2015, **44**:775–794.
32. Huang D, Wang G. Regional-specific spatial cross-correlation model for stochastic simulation of ground-motion time histories. *Bulletin of the Seismological Society of America* 2015, **105**(1):272–284.
33. Yeh CH, Wen YK. Modeling of nonstationary ground motion and analysis of inelastic structural response. *Structural Safety* 1990, **8**:281–298.
34. Yamamoto Y. Stochastic model for earthquake ground motion using wavelet packets. Ph.D. Thesis, Department of Civil and Environmental Engineering, Stanford University, Stanford, California, 2011.
35. Arias A. *Measure of Earthquake Intensity*, in: *Seismic Design for Nuclear Power Plants*, (Hansen RJ Ed.). Massachusetts Institute of Technology Press: Cambridge, Massachusetts, 1970. p. 438–483.
36. Bora SS, Scherbaum F, Kuehn N, Stafford P. On the relationship between Fourier and response spectra: implications for the adjustment of empirical ground-motion prediction equations (GMPes). *Bulletin of the Seismological Society of America* 2016, **106**(3):1235–1253.

37. Abrahamson NA. Non-stationary spectral matching. *Seismological Research Letters* 1992, **63**(1):30.
38. Silva WJ, Lee K. WES RASCAL code for synthesizing earthquake ground motions. State-of-the-Art for Assessing Earthquake Hazards in the United States. Report 24, U.S. Army Engineers Waterways Experiment Station, Misc. Paper S-73-1, 1987.
39. Hancock J, Watson-Lamprey J, Abrahamson NA, Bommer JJ, Markatis A, McCoy E, Mendis R. An improved method of matching response spectra of recorded earthquake ground motion using wavelets. *Journal of Earthquake Engineering* 2006, **10**:67–89.
40. Al Atik L, Abrahamson NA. An improved method for nonstationary spectral matching. *Earthquake Spectra* 2010, **26**(3):601–617.
41. Carlson C, Zekkos D, Athanasopoulos-Zekkos A, Hubler J. Impact of modification on ground motion characteristics and geotechnical seismic analyses for a California site. *Journal of Earthquake Engineering* 2014, **18**(5):696–713.
42. Du W, Wang G. A simple ground-motion prediction model for cumulative absolute velocity and model validation. *Earthquake Engineering & Structural Dynamics* 2013, **42**(8):1189–1202.
43. FEMA-356. Prestandard and commentary for the seismic rehabilitation of buildings. Federal Emergency Management Agency, Washington DC, USA, 2000.
44. Bradley BA. Correlation of significant duration with amplitude and cumulative intensity measures and its use in ground motion selection. *Journal of Earthquake Engineering* 2011, **15**(6):809–832.
45. Baker JW, Jayaram N. Correlation of spectral acceleration values from NGA ground motion models. *Earthquake Spectra* 2008, **24**(1):299–317.
46. Du W, Wang G. Prediction equations for ground-motion significant durations using the NGA-West2 database. *Bulletin of the Seismological Society of America* 2017, **107**(1):319–333.
47. Wang G, Du W. Empirical correlations between cumulative absolute velocity and spectral accelerations from NGA ground motion database. *Soil Dynamics and Earthquake Engineering* 2012, **43**:229–236.
48. Stafford PJ, Sgobba S, Marano GC. An energy-based envelope function for stochastic simulation of earthquake accelerograms. *Soil Dynamics and Earthquake Engineering* 2009, **29**:1123–1133.
49. Huang D. Stochastic simulation of spatially correlated earthquake time histories, and energy-compatible and spectrum-compatible ground motion modification using wavelet packets. Ph.D. thesis, Hong Kong University of Science and Technology, 2016.